Near-Ideal Dechirper for Plasma-Based Electron and Positron Acceleration Using a Hollow Channel Plasma

Y.P. Wu,[1] J.F. Hua,[1,*] C.-H. Pai,[1] W. An,[2] Z. Zhou,[1] J. Zhang,[1] S. Liu,[1] B. Peng,[1] Y. Fang,[1] S.Y. Zhou,[1] X.L. Xu,[3] C.J. Zhang,[4] F. Li,[4] Z. Nie,[4] W. Lu,[1,†] W.B. Mori,[4] and C. Joshi[4]

[1] *Key Laboratory of Particle and Radiation Imaging of Ministry of Education, Department of Engineering Physics, Tsinghua University, Beijing 100084, China*
[2] *Beijing Normal University, Beijing 100875, China*
[3] *SLAC National Accelerator Laboratory, Stanford, California 94309, USA*
[4] *University of California Los Angeles, Los Angeles, California 90095, USA*

(Received 3 August 2019; revised manuscript received 18 October 2019; published 4 December 2019)

Plasma-based electron or positron wakefield acceleration has made great strides in the past decade. Currently, one major challenge for its applications to coherent light sources and colliders is the relatively large energy spread (few-percent level) of the accelerated beams. This energy spread is usually dominated by a longitudinally correlated energy chirp induced by the wakefield. It is highly desirable to have a systematic method for reducing this spread to $\lesssim 0.1\%$ and, at the same time, maintaining the beam emittance. Here, a near-ideal dechirper based on a low-density hollow channel plasma is proposed and tested through large-scale three-dimensional particle-in-cell simulations. The theoretical analyses and simulations confirm that the positively correlated energy spread (chirp) of the electron or positron beam from a plasma accelerator can be significantly reduced by its self-wake in the hollow plasma channel from a few percent down to $\lesssim 0.1\%$ without noticeable beam emittance growth. Such a near-ideal dechirper may significantly improve the beam quality of plasma-based accelerators; thus paving the way for their applications to future compact free-electron lasers and colliders.

DOI: 10.1103/PhysRevApplied.12.064011

I. INTRODUCTION

A plasma wake driven by an intense laser pulse or a charged particle beam can be utilized to accelerate electrons and positrons at extremely large accelerating fields of about 100 GV/m, which are orders of magnitude larger than those in state-of-the-art radiofrequency microwave-based accelerators [1,2]. In the past decade, the field of plasma-based wakefield acceleration has reached several key milestones, such as multi-GeV electron acceleration in laser-driven wakes [3–11], and high-energy high-efficiency electron or positron acceleration in beam-driven wakes [12–15]; thus showing its potential for application in compact X-ray free-electron lasers (X-FELs) and linear colliders for particle physics. For these challenging applications, beams with both low emittance and low energy spread are required. For beam emittance, currently sub-μm rad emittance is measured [16,17] in laser wakefield acceleration experiments, and studies on controlled injection schemes also show the potential of generating beams with much lower emittance [18–21]. For the energy spread, however, current experiments can only produce beams with percent-level energy spread, and this is about one order of magnitude larger than that required for X-FELs and colliders. Therefore, it is critical to find systematic solutions for reducing the beam energy spread down to 0.1 % or lower.

Before one can invent ways to reduce the energy spread, it is imperative to understand where the energy spread comes from. To obtain high gradients, the plasma accelerator must be operated in a high-density plasma, which, in turn, means that the wavelength of the accelerating structure is microscopic (tens to hundreds of micrometers). Due to the very short wavelength of this structure, the acceleration phase interval occupied by the short electron or positron beam is much larger than that in a traditional accelerator. This can lead to a significant energy chirp in the beam, unless ideal beam loading can be achieved [22,23]. This chirp is typically much larger than the intrinsic slice energy spread of the beam. For example, in many recently proposed injection schemes, the intrinsic energy spread of the beam slices could be reduced to about 1 MeV or even to the tens of keV level [19–21,24,25]; therefore, for beam energies of more than a few hundred MeV, the energy chirp induced by the acceleration phase

*jfhua@tsinghua.edu.cn
†weilu@tsinghua.edu.cn

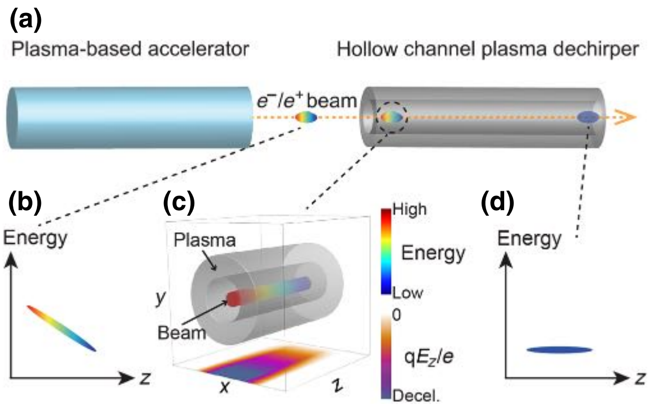

FIG. 1. Schematic diagram of a near-ideal hollow channel plasma dechirper. (a) A positively chirped electron or positron beam is generated in a plasma accelerator first, and then sent through a hollow channel plasma to dechirp itself. (b) The initial beam longitudinal phase space. (c) The longitudinal wakefield E_z excited by the beam in the hollow channel plasma. The projection in the $x-z$ plane shows the slice of qE_z/e at the midplane in the y direction, where q is the particle charge ($-e$ for electron and $+e$ for positron). (d) The final beam longitudinal phase space.

variance becomes the dominant part of the total energy spread.

To reduce the relatively large energy chirp in plasma accelerators, energy dechirpers based on tenuous uniform plasmas have recently been proposed and demonstrated [26–29], and phase space measurements clearly show the energy-spread-reduction effectiveness of such dechirpers [27]. However, this approach has a limitation for maintaining emittances well below about 1 μm rad due to longitudinal-position-dependent transverse wakefield focusing, and this effect is especially severe for positron beams. In addition, dechirping in a uniform plasma also induces a slice energy spread increase due to the nonuniform longitudinal wakefield in the transverse dimensions. These two factors impose restrictions for its application to X-FELs and linear colliders. Ideally, a dechirper that can both remove the energy chirp and maintain the emittance is preferred. Here, we propose to use a low-density hollow channel plasma to serve as such a near-ideal dechirper, as shown in Fig. 1(a).

In this scheme, a beam with a nearly linear positive energy chirp [Fig. 1(b); the beam energy increases quasi-linearly from head to tail, which is normal for an underloaded wake in a plasma accelerator [19,30]] is sent through a separate low-density hollow channel plasma section to excite a nearly linear plasma wake [Fig. 1(c)]. If the wake wavelength is much longer than the bunch length, the beam will entirely remain in a decelerating phase of the wake with a negative slope (the tail of the beam experiences a greater decelerating field than the head) inside the channel. Such a decelerating wake can effectively reduce the beam positive chirp during propagation [Fig. 1(d)]. The total dechirping effects can be easily tuned by changing the density, length, and geometry (i.e., inner and outer radii) of the plasma channel. If the parameters are properly designed, an energy spread reduction to the 0.1% level, or even lower, is indeed possible. At the same time, transverse focusing fields inside the channel will be zero, or negligibly small, if the beam is launched on or very close to the axis, and this will help to preserve the beam emittance [31]. We also note that this scheme works equally well for electron and positron beams; this is a unique feature that is crucial for application to electron-positron colliders.

In Secs. II and III, detailed theoretical analyses and three-dimensional (3D) particle-in-cell (PIC) simulations are systematically presented to show the effectiveness of the scheme illustrated in Fig. 1 on energy-spread reduction down to the 0.1% level and emittance preservation.

II. CONCEPT AND PIC SIMULATION ILLUSTRATION

To illustrate the effectiveness of the hollow channel plasma dechirper, we show here one example through 3D PIC simulations using the code QUICKPIC [32–34]. In this example, a 4 GeV electron or positron beam with a 1% (rms) linear positive energy chirp and an intrinsic slice energy spread of 0.4 MeV (rms) is sent on-axis through a hollow channel plasma about 55 cm long. The beam has 1 nC charge with a high peak current of $I_b = 10$ kA (near-flat-top current profile), and low normalized emittance of $\epsilon_{nx,y} = 0.2$ μm rad. As we see later in Sec. III, energy chirps for other current profiles can also be removed, but not as completely as that for a flat-top pulse. These parameters are chosen to be comparable to the required high-quality beam parameters in a future linear collider design [35,36]. The hollow channel plasma has an inner radius of $a = 300$ μm, an outer radius of $b = 500$ μm, and an electron density of $n_p = 5 \times 10^{15}$ cm^{-3} within the annular plasma ring. By the end of the simulations, the relative rms energy spreads (δ_W) of both the electron and positron beams are dramatically reduced from 1% to about 0.02%, which is close to the intrinsic slice energy spread (0.01%). At the same time, the emittances of the beams remain almost unchanged. Therefore, the six-dimensional (6D) brightness of the beam [$B_{6D} = 2I_b/(\epsilon_{nx}\epsilon_{ny}\delta_W) \approx 2.5 \times 10^{18}$ Am^{-2} rad^{-2}/0.1%] is effectively enhanced by a factor of 50.

Details of the simulations are presented in Fig. 2. The initial densities of the plasma channel and the e^-/e^+ beam are plotted in Fig. 2(a). The beams have a transverse Gaussian profile, with $\sigma_{x,y} = 4.0$ μm, and a near-flat-top longitudinal current profile [Fig. 2(b)]. The longitudinal wakefields E_z in the hollow channel plasma excited by the e^- and e^+ beams are shown in Figs. 2(c) and 2(d), respectively. One can see that these two fields are very similar,

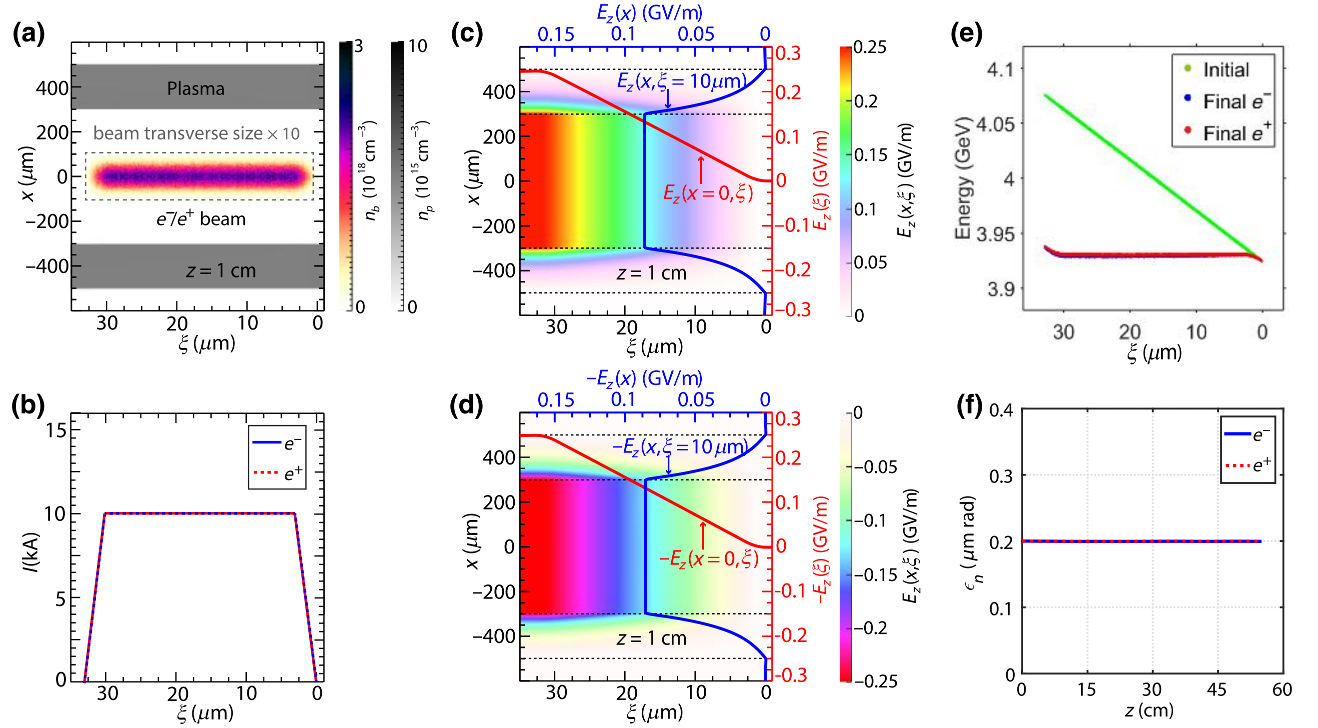

FIG. 2. 3D PIC simulations of the dechirping process in a hollow channel plasma. (a) The densities of the plasma channel (n_p) and the e^-/e^+ beam (n_b) in the $x-\xi$ plane when the propagation distance is $z=1$ cm. Here, $\xi = ct - z$ represents the longitudinal position relative to the beam head. (b) The e^-/e^+ beam current profile (a 90 fs long plateau and two 10 fs long ramps at each side). The E_z fields excited by the e^- (c) and e^+ (d) bunches, also at $z=1$ cm. The black dotted lines represent the inner and outer radii of the plasma channel. Line outs of the on-axis E_z ($x = 0$ μm, ξ) and radial variation in E_z (x, $\xi = 10$ μm) are separately shown with red and blue lines. (e) The longitudinal phase spaces of e^- and e^+ beams before and after the dechirper. (f) The evolutions of e^- and e^+ beam normalized emittances during the dechirping process.

except for a change of charge sign, and the on-axis line outs of both E_z fields have a near-linear deceleration along most of the beam length. The transverse uniformity of E_z within the channel can also be readily seen in Figs. 2(c) and 2(d). Combining the above two features of E_z, both beams (e^-/e^+) can be dechirped by the annular plasma with a negligible slice energy spread increase. After a propagation of 55.3 cm (e^-)/54.6 cm (e^+), the minimum rms energy spread of 0.76 MeV (e^-)/0.72 MeV (e^+) is achieved with a mean energy of 3.93 GeV. Thus, the relative rms energy spreads of the beams have been reduced from 1% to 0.019% (e^-)/0.018% (e^+). We note that the subtle differences between the e^- and e^+ beams come from the slightly different nonlinear plasma responses [37]. Figure 2(e) shows the corresponding longitudinal phase spaces of e^- and e^+ bunches before and after the dechirper. Clearly, the incoming linear energy chirp is removed, except at the very front and rear of the bunch. In Fig. 2(f), the evolutions of e^- and e^+ beam normalized emittances over the whole propagation are plotted, and it is evident that the emittances are well conserved.

To illustrate the differences between the hollow channel and recently proposed uniform plasma dechirper schemes, we also simulate the dechirping process of the same e^-/e^+ beam in a uniform plasma with a density identical to that in the above example. Figures 3(a) and 3(b) show the density distributions of the e^-/e^+ beam and the plasma. Due to such a high beam density ($n_b \gg n_p$), the plasma has a very different nonlinear response to the e^- and e^+ beams [38]. The e^- beam head blows plasma electrons away, and thus, its tail is located in an ion channel. In comparison, the e^+ beam sucks plasma electrons in, forming a highly dense electron sheath in the beam region. The resulting longitudinal wakefields E_z excited by the e^- and e^+ beams are shown in Figs. 3(c) and 3(d), respectively, where the longitudinal nonlinearity and transverse nonuniformity (especially for the e^+ case) of E_z are obvious. These two features will induce nonlinear energy chirp growth and a slice energy spread increase during the dechirping process. After propagation of 3.61 cm (e^-)/2.86 cm (e^+), a minimum rms energy spread of 11.58 MeV (e^-)/12.49 MeV (e^+) is obtained, which is about 15 (e^-)/17 (e^+) times larger than that achieved in the corresponding hollow channel plasma dechirper case. The longitudinal phase spaces of e^- and e^+ bunches before and after the dechirper are shown in Fig. 3(g), where the induced nonlinear energy chirp increase and slice energy spread growth are evident. Figures 3(e) and 3(f) show the transverse wakefields $W_\perp =$

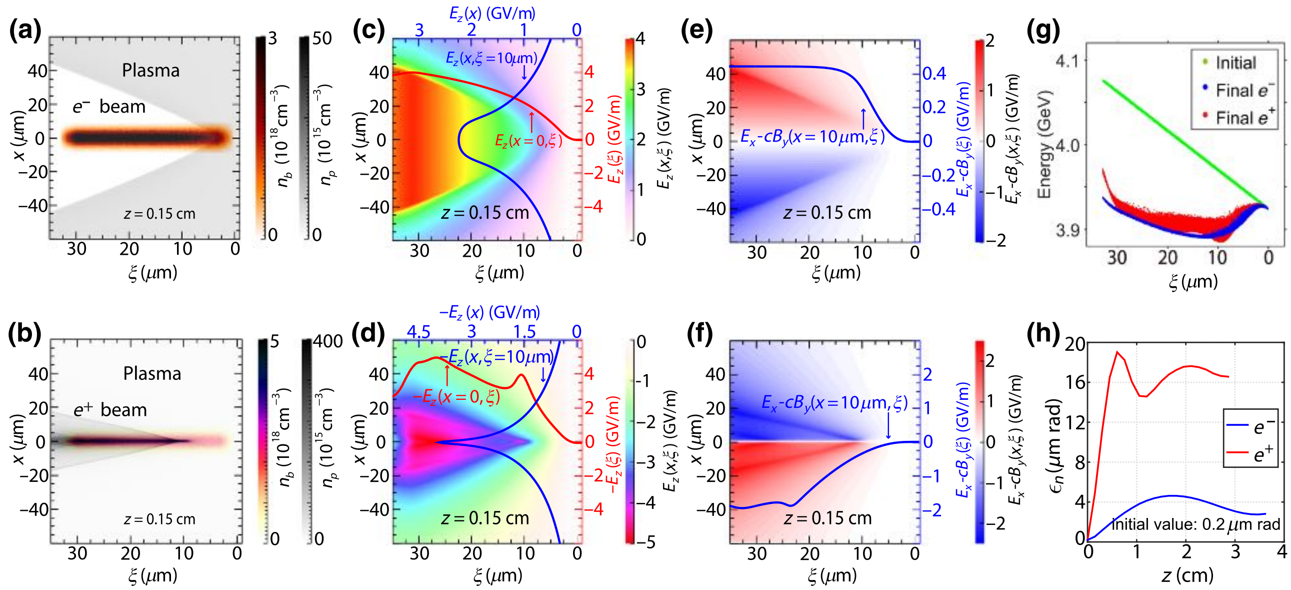

FIG. 3. 3D PIC simulations of the dechirping process in a uniform plasma. The densities of plasma (n_p) and beam (n_b) in the $x-\xi$ plane for e^- (a) and e^+ (b), at $z = 0.15$ cm. The E_z fields excited by the e^- (c) and e^+ (d) bunches, also at $z = 0.15$ cm. Line outs of the on-axis E_z ($x = 0$ μm, ξ) and radial variation in E_z (x, $\xi = 10$ μm) are separately shown with red and blue lines, respectively. The transverse wakefields $W_\perp = E_x - cB_y$ excited by the e^- (e) and e^+ (f) bunches, also at $z = 0.15$ cm. The line out of the off-axis $W_\perp$ ($x = 10$ μm, ξ) is shown with the blue line. (g) The longitudinal phase spaces of e^- and e^+ beams before and after the dechirper. (h) The evolutions of e^- and e^+ beam normalized emittances during the dechirping process.

$E_x - cB_y$ excited by the e^- and e^+ bunches, respectively. One can see that these two fields both depend on the longitudinal position, and thus, electrons at different longitudinal positions feel different focusing strengths and rotate with different velocities in the transverse phase space, leading to a large growth in projected emittance. In Fig. 3(h), the evolution of the e^-/e^+ beam normalized emittance over the whole propagation is plotted, and it is clear that the emittance has increased by a factor of 14 (e^-)/83 (e^+). Such enormous emittance growth is catastrophic for beam quality.

The above comparisons show that the hollow channel plasma dechirper scheme has a decisive advantage over the uniform plasma dechirper scheme in energy spread reduction and emittance preservation for high-brightness e^-/e^+ beams. Next, we analyze this concept in detail through theoretical analyses and 3D PIC simulations for various beam parameters.

III. THEORY AND PIC SIMULATION VERIFICATION

To quantify the effectiveness of the hollow channel plasma dechirper for various beam parameters, we carry out a theoretical analysis based on linear wakefield theory [22,39]. In the short bunch limit, where the wake wavelength is much larger than the beam bunch length, the plasma response to a narrow drive bunch in the hollow channel is relatively weak; therefore, the linear plasma wakefield theory can be adopted to properly describe the wakefield structure within the beam.

Using linear wakefield theory, the longitudinal wakefield E_z in the hollow channel excited by an on-axis cylindrically symmetric beam can be expressed as a convolution of the bunch charge distribution with a single-particle wakefunction [15,37,39]

$$E_z(r,\xi) = -\frac{q}{e}\frac{mk_p^2c^2}{e}A_0\int_{-\infty}^{\xi} d\xi' \cos[\Omega_0 k_p(\xi-\xi')]\frac{I(\xi')}{I_A}, \tag{1}$$

where m is the electron rest mass, $k_p = \sqrt{n_p e^2/m\varepsilon_0 c^2}$ is the plasma wave number, ε_0 is the vacuum permittivity, $I(\xi)$ is the beam current, and $I_A \approx 17$ kA is the Alfven current. In Eq. 1, A_0 and Ω_0 are two quantities related to the wake amplitude and wavelength,

$$A_0 = \frac{-4B_{00}(a,b)}{k_p a[2B_{10}(a,b) - k_p a B_{00}(a,b)]}, \tag{2}$$

$$\Omega_0 = \sqrt{\frac{2B_{10}(a,b)}{2B_{10}(a,b) - k_p a B_{00}(a,b)}}, \tag{3}$$

where $B_{ij}(a,b) = (-1)^{i-j+1}I_j(k_p b)K_i(k_p a) + I_i(k_p a)K_j(k_p b)$, and K_n and I_n are the modified Bessel functions of order n.

TABLE I. Dechirping effects for three typical current profiles[a].

	Flat top	Sin^2	Gaussian
$f(\xi)$	1	$\sin^2(\pi\xi/L_b)$	$e^{-(\xi-L_b/2)^2/[2(L_b/6)^2]}$ [b]
$E_z(r,\xi)$	$-\frac{q}{e}\frac{mk_p^2c^2}{e}A_0\frac{I_b}{I_A}\xi$	$-\frac{q}{e}\frac{mk_p^2c^2}{e}A_0\frac{I_b}{I_A}\left[\frac{\xi}{2}-\frac{L_b\sin(2\pi\xi/L_b)}{4\pi}\right]$	$-\frac{q}{e}\frac{mk_p^2c^2}{e}A_0\frac{I_b}{I_A}\sqrt{\frac{\pi}{72}}L_b\left[1+\mathrm{erf}\left(\frac{\xi-L_b/2}{\sqrt{2}L_b/6}\right)\right]$ [c]
G	$G_F=0$	$G_S\approx 0.139$	$G_G\approx 0.223$
H	$H_F\approx 3.464$	$H_S\approx 3.430$	$H_G\approx 3.377$

[a]The subscripts "F," "S," and "G" refer to the flat-top, sin^2, and Gaussian current profiles, respectively.
[b]The rms bunch length is assumed to be $L_b/6$.
[c]$\mathrm{erf}(\xi)=(2/\sqrt{\pi})\sum_{n=0}^{\infty}\{(-1)^n\xi^{2n+1}/[n!(2n+1)]\}$ is the Gauss error function.

In the short bunch limit ($k_pL_b \ll 1$), where L_b is the full bunch length, $\cos[\Omega_0 k_p(\xi-\xi')]$ reduces to 1; therefore, within the beam, Eq. (1) can be simplified as

$$E_z(r,\xi)\approx -\frac{q}{e}\frac{mk_p^2c^2}{e}A_0\frac{I_b}{I_A}\int_0^{\xi}d\xi' f(\xi'). \qquad (4)$$

Here, $f(\xi)$ is the normalized current profile. Equation (4) shows that E_z is a decelerating field with a negative slope for both e^- and e^+ beams. To quantify the dependence of E_z on the current profile, the expressions of E_z for three typical profiles (flat top, sin^2, and Gaussian) are calculated and listed in Table I (see Appendix A for details). For the flat-top current profile, E_z within the beam is exactly linear along ξ, which is ideal for completely removing a linear energy chirp. For non-flat-top profiles, nonlinear energy chirps will be induced; therefore, the final achievable minimum rms energy spread ΔW_f will be a trade-off between linear chirp reduction and nonlinear chirp growth.

ΔW_f and the required channel length, L_c, can be calculated as $\Delta W_f=\Delta W_i G$ and $L_c=(\Delta W_i/|qE_z(r,\xi=L_b)|)H$, where ΔW_i is the initial rms energy spread, $E_z(r,\xi=L_b)$ is the longitudinal electric field at the tail of the beam, and G and H are two geometrical factors determined by the beam current profile $f(\xi)$. The expressions of G and H for these three profiles are also listed in Table I (see Appendix A for details).

To verify the above theoretical expressions, a series of 3D PIC simulations using the code QUICKPIC have been performed. In these simulations, electron beams with different peak currents and profiles are initialized with zero slice energy spread and positive linear energy chirp (mean energy of 4 GeV and relative rms energy spread of 1%). The density of the annular plasma channel is $n_p=1\times 10^{17}$ cm^{-3}, with an inner radius of $a=30$ μm and an outer radius of $b=60$ μm.

Comparisons of the simulation results with theoretical expressions are shown in Figs. 4 and 5. Figures 4(a)–4(c) show very good agreement between the calculated and simulated E_z fields for three beam profiles (flat top, sin^2, and Gaussian) for a peak current of 10 kA. For lower beam currents, the agreement will be better due to a reduced nonlinear effect. The corresponding longitudinal phase spaces before and after the dechirper are shown in Figs. 4(d)–4(f). For the flat-top profile, the longitudinal phase space can be completely flattened, leading to a reduction in relative energy spread from 1% to below 0.01%. For the sin^2 and Gaussian profiles, E_z has a linear form for most of the beam, except at the bunch head and tail, where the nonlinear feature of the wakefield is evident. This nonlinearity results in a sigmoid structure in the final longitudinal phase space of the beam. Despite this nonideal feature, the relative energy spread can still be reduced significantly from 1% to 0.14% (sin^2)/0.22% (Gaussian).

The energy spread reductions versus propagation distances are plotted for these three different profiles in Figs. 5(a)–5(c). It can be clearly seen that the rms energy spread almost linearly decreases during beam propagation until the final minimum value is reached. For different peak currents, the achievable minimum rms energy spreads are almost the same for a given profile; this is in good accordance with linear wakefield theory analyses. In Figs. 5(d) and 5(e), the calculated and simulated G (which controls the final minimum energy spread, ΔW_f) and H (which controls the dechirping length, L_c) factors are also plotted, and excellent agreement is achieved.

As observed, a flat-top beam current profile has the best effect for linear energy chirp reduction, with a capability to obtain an energy spread well below 0.1%. Indeed, there are several possibilities in plasma-based acceleration for shaping the beam current profile through injection optimizations [19–21], and this is a very active research area.

IV. DISCUSSION

Sections II and III clearly demonstrate the effectiveness of a hollow channel plasma as a very effective dechirper. In practice, the robustness of this method should also be analyzed. A major factor that will derate the performance of this device is off-axis injection [40], which will excite a dipolelike transverse bending field that will steer the

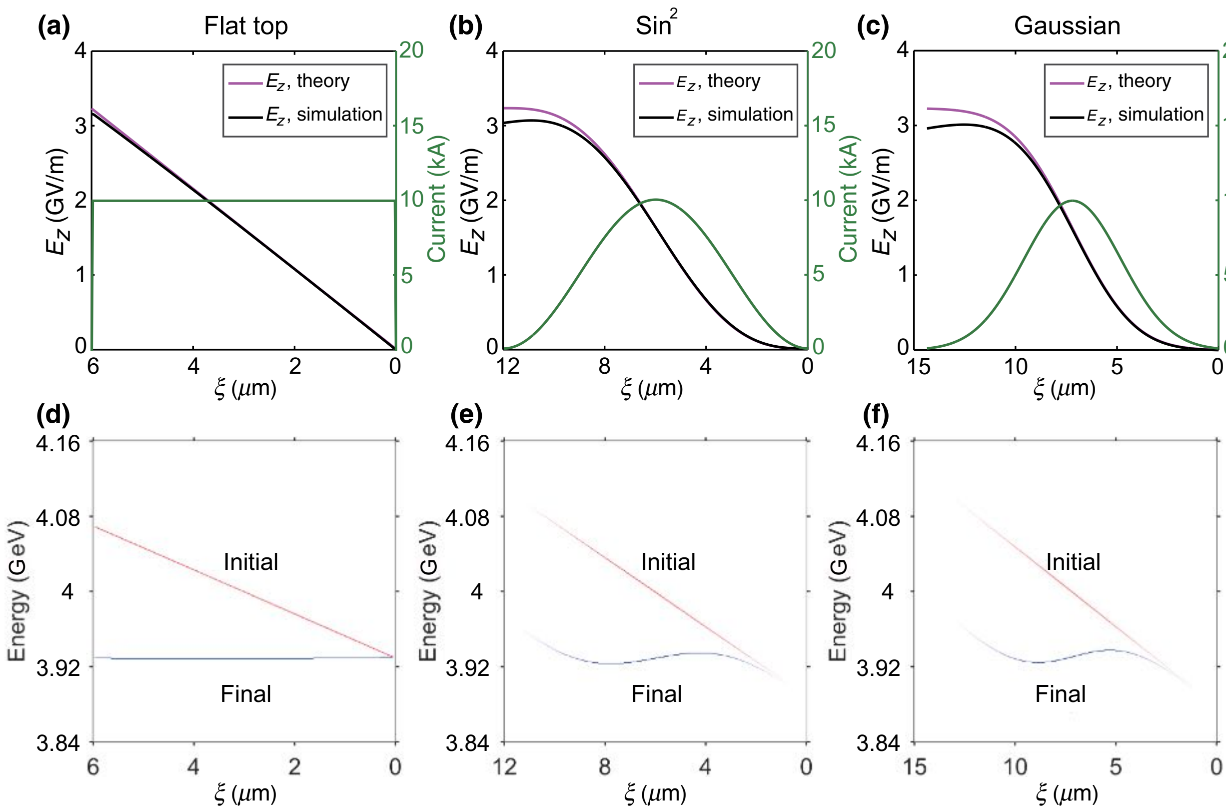

FIG. 4. Dechirping effects for three typical beam current profiles. Line outs of the calculated (in purple) and simulated (in black) E_z fields for flat-top (a), sin^2 (b), and Gaussian (c) current profiles. The corresponding beam longitudinal phase spaces before (in red) and after (in blue) the dechirper for flat-top (d), sin^2 (e), and Gaussian (f) current profiles. The beam parameters of bunch charge ($Q = 200$ pC), beam peak current ($I_b = 10$ kA), transverse beam size ($\sigma_{x,y} = 4\ \mu$m), and normalized emittance ($\epsilon_{nx,y} = 0.2\ \mu$m rad) are all the same for these three cases; these give the corresponding full bunch length L_b ($L_{b,F} = 6\ \mu$m for flat top, $L_{b,S} = 12\ \mu$m for sin^2, and $L_{b,G} \approx 14.4\ \mu$m for Gaussian).

beam towards one side. As a result of this deflection, the projected emittance of the beam in the direction of the offset will increase. To quantify the tolerance to off-axis injection, the transverse bending field, $W_\perp$, can be calculated for a given beam offset and current distribution [37, 40], and it turns out that $W_\perp$ is proportional to the offset, x_0. The value of $W_\perp$ also has a longitudinal dependence on the beam position; thus in the beam transverse phase space, slice phase ellipses develop a displacement with respect to each other, which leads to the projected emittance growth. In Fig. 6(a), the final longitudinal phase spaces are plotted for different initial beam offsets ($x_{0,i}$) using 3D PIC simulations. The beam and plasma parameters in this simulation and all subsequent simulations are identical to those in Fig. 2. As expected, a small relative offset has a negligible effect on the dechirping effects. Figure 6(b) shows the transverse beam offset growth and the relative beam projected emittance growth (in the direction of the offset) versus the initial beam offset. As observed, the beam offset growth is negligibly small compared with the channel inner radius, a, and the beam emittance growth can be controlled to less than about 25% for an initial beam offset within 2 μm. In addition to off-axis injection, a head-to-tail tilt on an on-axis beam will also lead to dipolelike transverse wakefields, which can induce slice-dependent emittance growth. In Fig. 6(c), the relative beam projected emittance growth (in the direction of the tilt) versus the initial angle of the linear tilt, $\theta_{x,i}$, is plotted via 3D PIC simulations. The beam emittance growth can be controlled to less than about 25% for $\theta_{x,i}$ within about 200 mrad. Furthermore, a transversely asymmetric beam (i.e., $\sigma_x \neq \sigma_y$) will also drive a quadrupolelike wake, even if it is on-axis injected and has no head-to-tail tilt [39]. Such a quadrupole wakefield will introduce longitudinal-position-dependent focusing or defocusing in the beam and increase the projected emittance. Using 3D PIC simulations, the relative beam projected emittance growth in both x and y directions versus the beam asymmetric ratio, $R_{\text{asym}} = \sigma_y/\sigma_x$ (keeping $\sigma_x\sigma_y$ fixed and assuming $\sigma_y > \sigma_x$), can be obtained. The results show that the beam emittance growth in both directions can be controlled to less than about 1% for R_{asym} within 4, which is a very relaxed tolerance. These simulation results suggest that the hollow channel plasma dechirper concept has a reasonably good tolerance for

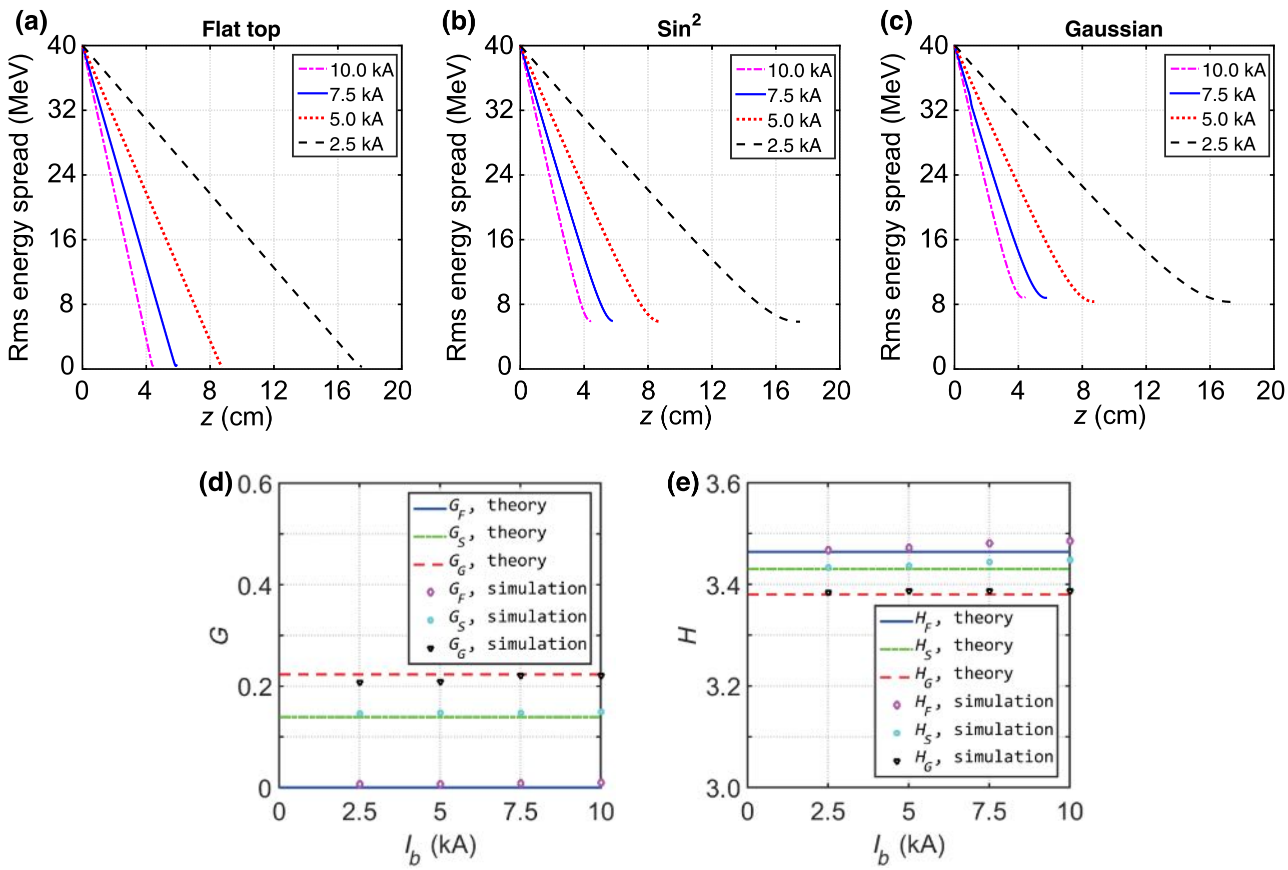

FIG. 5. The rms energy spread reductions versus propagation distances for flat-top (a), sin^2 (b), and Gaussian (c) beam profiles with different peak currents. The other parameters are identical to those in Fig. 4. The corresponding calculated and simulated geometrical factors G (d) and H (e) are given for these three current profiles.

all nonideal beam off-axis injection, head-to-tail tilt, and transverse asymmetry.

The performance of the hollow channel plasma dechirper also depends on the nonideal transverse shape of such a structure. Recent experiments have successfully demonstrated that an extended hollow plasma channel can be created by ionizing neutral gas with a high-order Bessel laser pulse [15,37,40]. In practice, due to possible

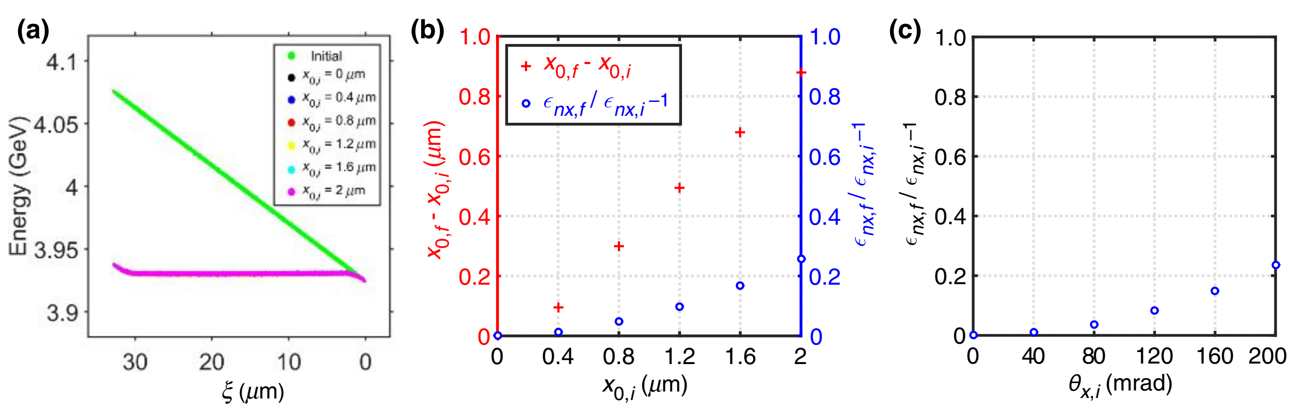

FIG. 6. (a) The initial and final longitudinal phase spaces of the beam for different initial beam offsets, $x_{0,i}$, obtained via 3D PIC simulations using the parameters given in Fig. 2. Regardless of the initial offset, the final longitudinal phase spaces are nearly the same. (b) The transverse offset growth of the beam centroid, $x_{0,f} - x_{0,i}$, and the projected normalized emittance growth, $\epsilon_{nx,f}/\epsilon_{nx,i} - 1$, versus the initial beam offset, $x_{0,i}$, where the subscripts "i" and "f" denote the initial and final quantities, respectively. (c) The projected normalized emittance growth, $\epsilon_{nx,f}/\epsilon_{nx,i} - 1$, versus the initial angle of the linear tilt, $\theta_{x,i}$. Notably, here the beam offset and tilt are both in the x direction.

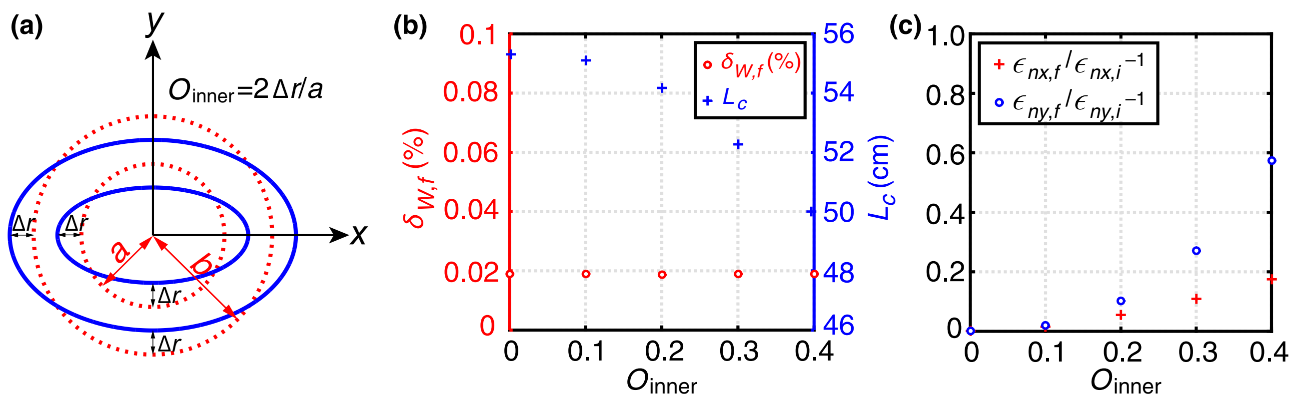

FIG. 7. Influence of channel transverse asymmetry on the dechirper performance. (a) The cross-sectional shape of a hollow plasma channel. The red dashed lines correspond to the boundaries of a perfectly circular ring, and the blue solid lines correspond to the boundaries of an area-equal elliptical ring. The definition of the ovality of the inner ellipse, O_{inner}, is also illustrated. (b) The final beam relative rms energy spread, $\delta_{W,f}$, and required channel length, L_c, versus O_{inner} are obtained via 3D PIC simulations using the parameters in Fig. 2. (c) The simulated projected normalized emittance growths $\epsilon_{nx,f}/\epsilon_{nx,i}-1$ and $\epsilon_{ny,f}/\epsilon_{ny,i}-1$ versus O_{inner}.

aberrations of the ionization laser, the cross-sectional shape of a realistic hollow plasma channel may be elliptical instead of perfectly circular [37]. Similar to the asymmetric beam case, a quadrupolelike wake will also be excited, even for an on-axis, no-tilt, and symmetric beam, leading to longitudinal-position-dependent focusing or defocusing, and thus, the projected emittance growth. Assuming the major (minor) axis of the elliptical ring is along the x (y) direction [see Fig. 7(a)], in Fig. 7(b) the final beam energy spread and required channel length versus the ovality of the inner ellipse, O_{inner} [defined as the length difference between the semimajor and semiminor axes of the inner ellipse divided by the ideal inner radius, a, as illustrated in Fig. 7(a)] are plotted via 3D PIC simulations. Although the required channel length slightly decreases with an increase in O_{inner}, the final beam energy spread remains almost unchanged. In Fig. 7(c), the simulated relative beam projected emittance growths in both x and y directions for different O_{inner} are plotted. As observed, the beam emittance growths in both directions can be controlled to less than about 25% for O_{inner} within 30%. This tolerance can be easily achieved for current experimental conditions.

In addition, a realistic hollow plasma channel may have a finite thickness of plasma wall [39,41]. Assuming the wall thickness, d [the distance over which the density changes linearly from zero to n_p, see Fig. 8(a)], is small compared with the channel inner or outer radius, a or b, 3D PIC simulations show that the decelerating field strength increases, and thus, the required channel length decreases as the channel becomes thicker [keeping a and b fixed; see Fig. 8(b)]. Even with this nonideal channel boundary, the final achievable minimum energy

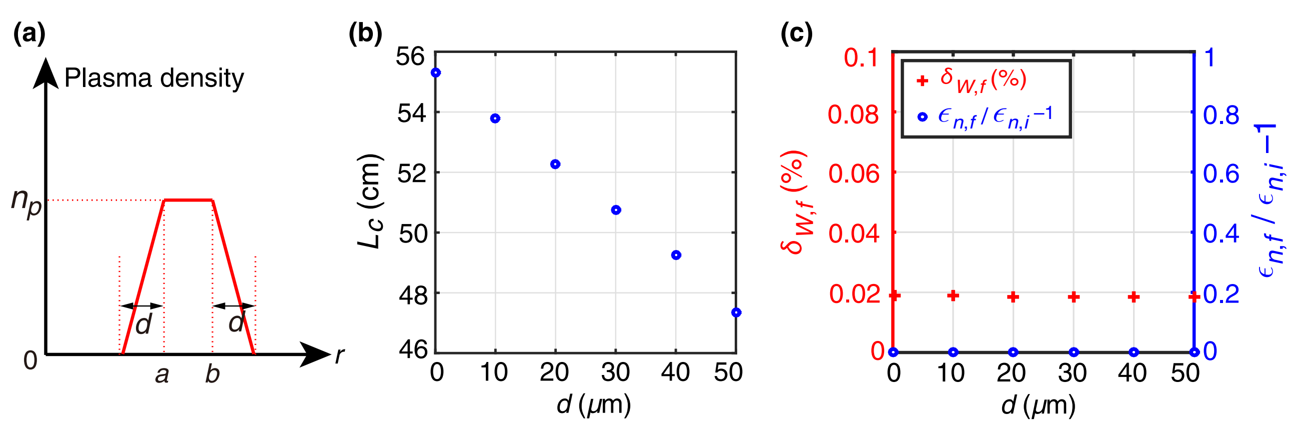

FIG. 8. Influence of finite-thickness plasma wall on the dechirper performance. (a) The plasma density distribution of a hollow channel with a finite-thickness wall. (b) The required plasma channel length, L_c, versus the plasma wall thickness, d, obtained via 3D PIC simulations using the parameters in Fig. 2. (c) The simulated final beam relative rms energy spread, $\delta_{W,f}$, and projected normalized emittance growth, $\epsilon_{n,f}/\epsilon_{n,i}-1$, versus the plasma wall thickness, d.

spread and the output beam emittance are nearly the same as those in the ideal step-function boundary case [see Fig. 8(c)].

V. SUMMARY

In summary, a method that uses a hollow channel plasma as a near-ideal dechirper to reduce the energy chirp of electron and positron beams in plasma-based accelerators is proposed. Theoretical analyses and 3D PIC simulations are systematically used to confirm the effectiveness and robustness of this method at reducing the beam energy spread from the few-percent level to about 0.1% or lower, while maintaining the beam's slice energy spread and normalized emittance. This tunable and flexible technique works well for both electron and positron beams, and it can be applied to future plasma-based photon sources and colliders to enhance significantly the beam 6D brightness.

ACKNOWLEDGMENTS

This work is supported by the National Natural Science Foundation of China (NSFC) (Grants No. 11535006, No. 11425521, No. 11775125, and No. 11875175), the CAS Center for Excellence in Particle Physics, and the U.S. Department of Energy (Grants No. DE-SC0010064, No. DE-SC0008491, and No. DE- SC0008316) at UCLA.

APPENDIX: CALCULATION OF E_z AND GEOMETRICAL FACTORS (G AND H) FOR THREE TYPICAL BEAM CURRENT PROFILES

To quantify the dechirping effectiveness, the evolution of the beam energy spread is derived for three typical current profiles (flat top, $\sin^2$, and Gaussian). For an electron or positron beam with a linear positive energy chirp and zero intrinsic slice energy spread, its initial energy profile can be expressed as $W(\xi, z=0) = W_{\text{head},i} + [(W_{\text{tail},i} - W_{\text{head},i})/L_b]\xi$, where $W_{\text{head},i}$ ($W_{\text{tail},i}$) is the initial energy of the beam head (tail). During the dechirping process, since the decelerating field, E_z, within the beam has no dependence on r, the beam energy distribution at the longitudinal position, z, can be written as $W(\xi, z) = W(\xi, z=0) + qE_z(\xi)z$. Thus, the mean energy and rms energy spread of the beam yield

$$W_{\text{mean}}(z) = \frac{\int_0^{L_b} W(\xi, z) f(\xi) d\xi}{\int_0^{L_b} f(\xi) d\xi}, \tag{A1}$$

and

$$\Delta W(z) = \sqrt{\frac{\int_0^{L_b} [W(\xi, z) - W_{\text{mean}}(z)]^2 f(\xi) d\xi}{\int_0^{L_b} f(\xi) d\xi}}. \tag{A2}$$

When $z = 0$, Eq. (A2) gives the initial rms energy spread, ΔW_i. The final minimum rms energy spread, ΔW_f, can be achieved when $d\Delta W(z)/dz = 0$, and the corresponding value of z is the required plasma dechirper length, L_c.

For the flat-top current profile, i.e., $f(\xi) = 1$ for $0 \le \xi \le L_b$. In accordance with Eq. (4), E_z within the beam is exactly linear along ξ,

$$E_z(\xi) = -\frac{q}{e} \frac{mk_p^2 c^2}{e} A_0 \frac{I_b}{I_A} \xi. \tag{A3}$$

Therefore, the linear energy chirp of the beam can be completely removed without inducing nonlinear energy chirp or slice energy spread, yielding zero ΔW_f, i.e., $G_F = 0$. The plasma dechirper length, $L_{c,F}$, can be intuitively obtained as $L_{c,F} = (W_{\text{tail},i} - W_{\text{head},i})/|qE_z(\xi = L_b)|$. Indeed, to make a comparison between different current profiles, we keep ΔW_i fixed. In this case, according to Eq. (A2), $W_{\text{tail},i} - W_{\text{head},i} \approx 3.464\Delta W_i$; therefore, $L_{c,F}$ can be rewritten in terms of ΔW_i,

$$L_{c,F} = \frac{\Delta W_i}{|qE_z(\xi = L_b)|} H_F = \frac{\Delta W_i}{mk_p^2 c^2 A_0 \frac{I_b}{I_A} L_b} H_F, \tag{A4}$$

where $H_F \approx 3.464$.

For the $\sin^2$ current profile, i.e., $f(\xi) = \sin^2(\pi\xi/L_b)$. According to Eq. (4), the expression for E_z is

$$E_z(\xi) = -\frac{q}{e} \frac{mk_p^2 c^2}{e} A_0 \frac{I_b}{I_A} \left[\frac{\xi}{2} - \frac{L_b \sin(2\pi\xi/L_b)}{4\pi}\right], \tag{A5}$$

One can see the first term in brackets is the linear term of ξ, while the second term is the high-order nonlinear correction, which leads to the nonlinear energy chirp growth. After obtaining an expression for $\Delta W(z)$ and setting $d\Delta W(z)/dz = 0$, we find $G_S \approx 0.139$ and $L_{c,S} \approx (W_{\text{tail},i} - W_{\text{head},i})/|qE_z(\xi = L_b)| \times 0.6201$. Based on Eq. (A2), $W_{\text{tail},i} - W_{\text{head},i} \approx 5.532\Delta W_i$; thus $L_{c,s}$ yields

$$L_{c,S} = \frac{\Delta W_i}{|qE_z(\xi = L_b)|} H_S = \frac{\Delta W_i}{mk_p^2 c^2 A_0 \frac{I_b}{I_A} \frac{L_b}{2}} H_S, \tag{A6}$$

where $H_S \approx 0.6201 \times 5.532 \approx 3.430$.

For the Gaussian current profile, the beam is assumed to be cut off outside three standard deviations from the beam center, i.e., $f(\xi) = e^{-(\xi - L_b/2)^2/[2(L_b/6)^2]}$. Substituting $f(\xi)$ into Eq. (4), E_z within the beam can be expressed as

$$E_z(\xi) = -\frac{q}{e} \frac{mk_p^2 c^2}{e} A_0 \frac{I_b}{I_A} \sqrt{\frac{\pi}{72}} L_b \left[1 + \text{erf}\left(\frac{\xi - L_b/2}{\sqrt{2} L_b/6}\right)\right]. \tag{A7}$$

Since the Gauss error function has both linear and nonlinear terms, the high-order nonlinear energy chirp will increase during the dechirping process. Similar to the $\sin^2$ current profile case, we can obtain $G_G \approx 0.223$ and $L_{c,G} \approx$

$(W_{\text{tail},i} - W_{\text{head},i})/|qE_z(\xi = L_b)| \times 0.5553$. From Eq. (A2), we have $W_{\text{tail},i} - W_{\text{head},i} \approx 6.081\Delta W_i$; hence $L_{c,G}$ is given by

$$L_{c,G} = \frac{\Delta W_i}{|qE_z(L_b)|} H_G = \frac{\Delta W_i}{mk_p^2 c^2 A_0 \frac{I_b}{I_A} \sqrt{2\pi} L_b/6} H_G, \quad \text{(A8)}$$

where $H_G \approx 0.5553 \times 6.081 \approx 3.377$.

[1] T. Tajima and J. M. Dawson, Laser Electron Accelerator, Phys. Rev. Lett. **43**, 267 (1979).

[2] Pisin Chen, J. M. Dawson, Robert W. Huff, and T. Katsouleas, Acceleration of Electrons by the Interaction of a Bunched Electron Beam with a Plasma, Phys. Rev. Lett. **54**, 693 (1985).

[3] S. P. D. Mangles, C. D. Murphy, Z. Najmudin, A. G. R. Thomas, J. L. Collier, A. E. Dangor, E. J. Divall, P. S. Foster, J. G. Gallacher, C. J. Hooker, D. A. Jaroszynski, A. J. Langley, W. B. Mori, P. A. Norreys, F. S. Tsung, R. Viskup, B. R. Walton, and K. Krushelnick, Monoenergetic beams of relativistic electrons from intense laser-plasma interactions, Nature **431**, 535 (2004).

[4] C. G. R. Geddes, Cs. Toth, J. van Tilborg, E. Esarey, C. B. Schroeder, D. Bruhwiler, C. Nieter, J. Cary, and W. P. Leemans, High-quality electron beams from a laser wakefield accelerator using plasma-channel guiding, Nature **431**, 538 (2004).

[5] J. Faure, Y. Glinec, A. Pukhov, S. Kiselev, S. Gordienko, E. Lefebvre, J.-P. Rousseau, F. Burgy, and V. Malka, A laser-plasma accelerator producing mono energetic electron beams, Nature **431**, 541 (2004).

[6] W. P. Leemans, B. Nagler, A. J. Gonsalves, Cs. Toth, K. Nakamura, C. G. R. Geddes, E. Esarey, C. B. Schroeder, and S. M. Hooker, Gev electron beams from a centimetre-scale accelerator, Nat. Phys. **2**, 696 (2006).

[7] Nasr A. M. Hafz, Tae Moon Jeong, Il Woo Choi, Seong Ku Lee, Ki Hong Pae, Victor V. Kulagin, Jae Hee Sung, Tae Jun Yu, Kyung-Han Hong, Tomonao Hosokai, John R. Cary, Do-Kyeong Ko, and Jongmin Lee, Stable generation of gev-class electron beams from self-guided laser-plasma channels, Nat. Photonics **2**, 571 (2008).

[8] Xiaoming Wang *et al.*, Quasi-monoenergetic laser-plasma acceleration of electrons to 2gev, Nat. Commun. **4**, 1988 (2013).

[9] Hyung Taek Kim, Ki Hong Pae, Hyuk Jin Cha, I. Jong Kim, Tae Jun Yu, Jae Hee Sung, Seong Ku Lee, Tae Moon Jeong, and Jongmin Lee, Enhancement of Electron Energy to the Multi-gev Regime by a Dual-stage Laser-wakefield Accelerator Pumped by Petawatt Laser Pulses, Phys. Rev. Lett. **111**, 165002 (2013).

[10] W. P. Leemans, A. J. Gonsalves, H.-S. Mao, K. Nakamura, C. Benedetti, C. B. Schroeder, Cs. Toth, J. Daniels, D. E. Mittelberger, S. S. Bulanov, J.-L. Vay, C. G. R. Geddes, and E. Esarey, Multi-gev Electron Beams from Capillary-discharged-guided Subpetawatt Laser Pulses in the Self-trapping Regime, Phys. Rev. Lett. **113**, 245002 (2014).

[11] A. J. Gonsalves *et al.*, Petawatt Laser Guiding and Electron Beam Acceleration to 8 gev in a Laser-heated Capillary Discharge Waveguide, Phys. Rev. Lett. **122**, 084801 (2019).

[12] Ian Blumenfeld, Christopher E. Clayton, Franz-Josef Decker, Mark J. Hogan, Chengkun Huang, Rasmus Ischebeck, Richard Iverson, Chandrashekhar Joshi, Thomas Katsouleas, Neil Kirby, Wei Lu, Kenneth A. Marsh, Warren B. Mori, Patric Muggli, Erdem Oz, Robert H. Siemann, Dieter Walz, and Miaomiao Zhou, Energy doubling of 42 gev electrons in a metre-scale plasma wakefield accelerator, Nature **445**, 741 (2007).

[13] M. Litos *et al.*, High-efficiency acceleration of an electron beam in a plasma wakefield accelerator, Nature **515**, 92 (2014).

[14] S. Corde *et al.*, Multi-gigaelectronvolt acceleration of positrons in a self-loaded plasma wakefield, Nature **524**, 442 (2015).

[15] Spencer Gessner *et al.*, Demonstration of a positron beam-driven plasma wakefield accelerator, Nat. Commun. **7**, 11785 (2016).

[16] R. Weingartner, S. Raith, A. Popp, S. Chou, J. Wenz, K. Khrennikov, M. Heigoldt, A. R. Maier, N. Kajumba, M. Fuchs, B. Zeitler, F. Krausz, S. Karsch, and F. Grüner, Ultralow emittance electron beams from a laser-wakefield accelerator, Phys. Rev. ST Accel. Beams **15**, 111302 (2012).

[17] S. K. Barber, J. van Tilborg, C. B. Schroeder, R. Lehe, H.-E. Tsai, K. K. Swanson, S. Steinke, K. Nakamura, C. G. R. Geddes, C. Benedetti, E. Esarey, and W. P. Leemans, Measured Emittance Dependence on the Injection Method in Laser Plasma Accelerators, Phys. Rev. Lett. **119**, 104801 (2017).

[18] B. Hidding, G. Pretzler, J. B. Rosenzweig, T. Königstein, D. Schiller, and D. L. Bruhwiler, Ultracold Electron Bunch Generation via Plasma Photocathode Emission and Acceleration in a Beam-driven Plasma Blowout, Phys. Rev. Lett. **108**, 035001 (2012).

[19] F. Li, J. F. Hua, X. L. Xu, C. J. Zhang, L. X. Yan, Y. C. Du, W. H. Huang, H. B. Chen, C. X. Tang, W. Lu, C. Joshi, W. B. Mori, and Y. Q. Gu, Generating High-brightness Electron Beams via Ionization Injection by Transverse Colliding Lasers in a Plasma-wakefield Accelerator, Phys. Rev. Lett. **111**, 015003 (2013).

[20] X. L. Xu, Y. P. Wu, C. J. Zhang, F. Li, Y. Wan, J. F. Hua, C.-H. Pai, W. Lu, P. Yu, C. Joshi, and W. B. Mori, Low emittance electron beam generation from a laser wakefield accelerator using two laser pulses with different wavelengths, Phys. Rev. ST Accel. Beams **17**, 061301 (2014).

[21] X. L. Xu, F. Li, W. An, T. N. Dalichaouch, P. Yu, W. Lu, C. Joshi, and W. B. Mori, High quality electron bunch generation using a longitudinal density-tailored plasma-based accelerator in the three-dimensional blowout regime, Phys. Rev. ST Accel. Beams **20**, 111303 (2017).

[22] T. Katsouleas, S. Wilks, P. Chen, J. M. Dawson, and J. J. Su, Beam loading in plasma accelerators, Part. Accel. **22**, 81 (1987).

[23] M. Tzoufras, W. Lu, F. S. Tsung, C. Huang, W. B. Mori, T. Katsouleas, J. Vieira, R. A. Fonseca, and L. O. Silva,

Beam Loading in the Nonlinear Regime of Plasma-based Acceleration, Phys. Rev. Lett. **101**, 145002 (2008).

[24] F. Li, C. J. Zhang, Y. Wan, Y. P. Wu, X. L. Xu, J. F. Hua, C.-H. Pai, W. Lu, Y. Q. Gu, W. B. Mori, and C. Joshi, Low-energy-spread laser wakefield acceleration using ionization injection with a tightly focused laser in a mismatched plasma channel, Plasma Phys. Control. Fusion **58**, 034004 (2016).

[25] Y. Wan, C. J. Zhang, F. Li, Y. P. Wu, J. F. Hua, C.-H. Pai, W. Lu, Y. Q. Gu, X. L. Xu, C. Joshi, and W. B. Mori, Colliding ionization injection in a plasma wakefield accelerator, Plasma Phys. Control. Fusion **58**, 034015 (2016).

[26] Y. P. Wu, Y. C. Du, J. Zhang, Z. Zhou, Z. Cheng, S. Zhou, J. Hua, C. Pai, and W. Lu, in *Proceedings of IPAC 2017, Copenhagen, Denmark* (Joint Accelerator Conferences Website, Copenhagen, 2017), p. 1258.

[27] Y. P. Wu, J. F. Hua, Z. Zhou, J. Zhang, S. Liu, B. Peng, Y. Fang, Z. Nie, X. N. Ning, C.-H. Pai, Y. C. Du, W. Lu, C. J. Zhang, W. B. Mori, and C. Joshi, Phase Space Dynamics of a Plasma Wakefield Dechirper for Energy Spread Reduction, Phys. Rev. Lett. **122**, 204804 (2019).

[28] R. D'Arcy *et al.*, Tunable Plasma-based Energy Dechirper, Phys. Rev. Lett. **122**, 034801 (2019).

[29] V. Shpakov *et al.*, Longitudinal Phase-space Manipulation with Beam-driven Wakefields, Phys. Rev. Lett. **122**, 114801 (2019).

[30] G. G. Manahan, A. F. Habib, P. Scherkl, P. Delinikolas, A. Beaton, A. Knetsch, O. Karger, G. Wittig, T. Heinemann, Z. M. Sheng, J. R. Cary, D. L. Bruhwiler, J. B. Rosenzweig, and B. Hidding, Single-stage plasma-based correlated energy spread compensation for ultrahigh 6d brightness electron beams, Nat. Commun. **8**, 15705 (2017).

[31] T. C. Chiou and T. Katsouleas, High Beam Quality and Efficiency in Plasma-based Accelerators, Phys. Rev. Lett. **81**, 3411 (1998).

[32] C. Huang, V. K. Decyk, C. Ren, M. Zhou, W. Lu, W. B. Mori, J. H. Cooley, T. M. Antonsen, Jr., and T. Katsouleas, Quickpic: A highly efficient fully parallelized pic code for plasma-based acceleration, J. Phys. Confer. Ser. **46**, 190 (2006).

[33] Weiming An, Viktor K. Decyk, Warren B. Mori, and Thomas M. Antonsen, Jr., An improved iteration loop for the three dimensional quasi-static particle-in-cell algorithm: Quickpic, J. Comput. Phys. **250**, 165 (2013).

[34] Quickpic open source, https://github.com/UCLA-Plasma-Simulation-Group/QuickPIC-OpenSource.

[35] The International Linear Collider Technical Design Report (2013), http://www.linearcollider.org/ILC/Publications/Techinical-Design-Report.

[36] C. B. Schroeder, E. Esarey, C. G. R. Geddes, C. Benedetti, and W. P. Leemans, Physics considerations for laser-plasma linear colliders, Phys. Rev. Spec. Top. Accel. Beams **13**, 101301 (2010).

[37] S. Gessner, Ph.D. thesis, School Stanford University, 2016.

[38] W. Lu, C. Huang, M. M. Zhou, W. B. Mori, and T. Katsouleas, Limits of linear plasma wakefield theory for electron or positron beams, Phys. Plasmas **12**, 063101 (2005).

[39] C. B. Schroeder, D. H. Whittum, and J. S. Wurtele, Multimode Analysis of the Hollow Plasma Channel Wakefield Accelerator, Phys. Rev. Lett. **82**, 1177 (1999).

[40] C. A. Lindstrøm *et al.*, Measurement of Transverse Wakefields Induced by a Misaligned Positron Bunch in a Hollow Channel Plasma Accelerator, Phys. Rev. Lett. **120**, 124802 (2018).

[41] A. Pukhov, O. Jansen, T. Tueckmantel, J. Thomas, and I. Yu. Kostyukov, Field-reversed Bubble in Deep Plasma Channels for High-quality Electron Acceleration, Phys. Rev. Lett. **113**, 245003 (2014).